CHEMISTRY
A EUROPEAN JOURNAL

DOI: 10.1002/chem.200601339

Carbon Dioxide Hydrogenation Catalyzed by a Ruthenium Dihydride: A DFT and High-Pressure Spectroscopic Investigation

Atsushi Urakawa,[a] Fabian Jutz,[a] Gábor Laurenczy,[b] and Alfons Baiker*[a]

Abstract: Reaction pathways during CO_2 hydrogenation catalyzed by the Ru dihydride complex $[Ru(dmpe)_2H_2]$ ($dmpe = Me_2PCH_2CH_2PMe_2$) have been studied by DFT calculations and by IR and NMR spectroscopy up to 120 bar in toluene at 300 K. CO_2 and formic acid readily inserted into or reacted with the complex to form formates. Two formate complexes, *cis*-$[Ru(dmpe)_2(OCHO)_2]$ and *trans*-$[Ru(dmpe)_2H(OCHO)]$, were formed at low CO_2 pressure (<5 bar). The latter occurred exclusively when formic acid reacted with the complex. A RuH···HOCHO dihydrogen-bonded complex of the *trans* form was identified at H_2 partial pressure higher than about 50 bar. The *trans* form of the complex is suggested to play a pivotal role in the reaction pathway. Potential-energy profiles along possible reaction paths have been investigated by static DFT calculations, and lower activation-energy profiles via the *trans* route were confirmed. The H_2 insertion has been identified as the rate-limiting step of the overall reaction. The high energy of the transition state for H_2 insertion is attributed to the elongated Ru–O bond. The H_2 insertion and the subsequent formation of formic acid proceed via $Ru(\eta^2\text{-}H_2)$-like complexes, in which apparently formate ion and Ru^+ or $Ru(\eta^2\text{-}H_2)^+$ interact. The bond properties of involved Ru complexes were characterized by natural bond orbital analysis, and the highly ionic characters of various complexes and transition states are shown. The stability of the formate ion near the Ru center likely plays a decisive role for catalytic activity. Removal of formic acid from the dihydrogen-bonded complex (RuH···HOCHO) seems to be crucial for catalytic efficiency, since formic acid can easily react with the complex to regenerate the original formate complex. Important aspects for the design of highly active catalytic systems are discussed.

Keywords: carbon dioxide fixation · density functional calculations · high-pressure chemistry · hydrogenation · ruthenium

Introduction

The use of industrially produced CO_2 as a chemical feedstock is gaining growing attention, driven by environmental,[1] legal,[2] and social factors.[3] Atmospheric CO_2 is a major contributor to the greenhouse effect, and various strategies have been developed for lowering its concentration in the atmosphere.[4] Although the use of CO_2 in chemical synthesis[4–8] contributes relatively little to mitigation of the CO_2 concentration in the atmosphere, several other factors render CO_2 an interesting chemical feedstock, such as high abundance, relative nontoxicity, low cost, and low critical temperature. A variety of products can be synthesized from CO_2[4,6–8] and among them formic acid derivatives have gained particular attention.

Syntheses of formic acid,[9–15] various alkyl formates,[9,15,16] and formamides[15,17–19] utilizing gaseous CO_2 and H_2 with mainly homogeneous transition-metal catalysts have been reported since the mid-1970s. An important breakthrough was reported by Noyori and co-workers in the mid-1990s.[14,15,17,18] By using supercritical CO_2 as both reactant and solvent, high turnover frequencies of the reactions were achieved. The high diffusivity of gases, weak catalyst solvation, and the high solubility of H_2 in supercritical CO_2 were attributed to be at the origin of the high turnovers.[15] The work of Noyori and co-workers clearly indicates that alkyl formates or formamides are formed consecutively after formic acid by reaction of formic acid with alcohol or

[a] Dr. A. Urakawa, F. Jutz, Prof. Dr. A. Baiker
Institute for Chemical and Bioengineering
Department of Chemistry and Applied Biosciences, ETH Zurich
Hönggerberg, HCI, 8093 Zurich (Switzerland)
Fax: (+41) 44-632-1163
E-mail: baiker@chem.ethz.ch

[b] Dr. G. Laurenczy
Institut des Sciences et Ingénierie Chimiques
Ecole Polytechnique Fédérale de Lausanne
BCH, 1015 Lausanne (Switzerland)

Supporting information for this article is available on the WWW under http://www.chemeurj.org/ or from the author.

amine, respectively.[15] In other words, formation of formic acid by hydrogenation of CO_2 seems to be the common pathway and plays a critical role in the activity of the three different reaction systems besides other effects such as promoter and solvent. Hence, elucidation of the pathways of formic acid formation is expected to lead to understanding of reaction systems in which CO_2 and H_2 are involved and also explain effects of different ligands and additives. Theoretical investigations have so far concluded that CO_2 insertion is the rate-limiting step[20,21] or that the reaction rate does not depend on H_2 pressure,[22] in spite of the fact that strong dependence of the reaction rate on H_2 pressure has been reported for homogeneous[12,15,23] and immobilized heterogeneous catalysts.[24]

In the present work, we studied the reaction pathways during CO_2 hydrogenation spectroscopically by high-pressure IR and high-pressure NMR spectroscopy and theoretically by DFT for $[Ru(dmpe)_2H_2]$ (dmpe = $Me_2PCH_2CH_2PMe_2$) as catalyst. This combined approach enhances the reliability of the theoretical models by excluding complexes that are irrelevant in practice. $[Ru(dmpe)_2H_2]$ was chosen because of its activity in the reaction,[15] simple identification of spectra, and faster convergence in the theoretical geometry optimization due to its rigid framework afforded by the ethylene bridge of the ligand. The size of the catalyst allows modeling of the full catalytic system with minimum assumptions. CO_2 insertion has also been studied by Perutz and co-workers using NMR spectroscopy, and various intermediate complexes have been identified.[25] This study serves as a reference for our work. Toluene was used as a solvent to attain reasonable concentration for spectroscopic measurements with clear proof that the reaction can proceed in apolar solvents such as benzene under high CO_2 and H_2 pressure.[26] High pressure, especially of H_2, is necessary to achieve a high reaction rate by increasing H_2 concentration in solutions; therefore, the spectra were measured under high H_2 pressure (up to 120 bar). As will be shown, significant changes occur in the state of the catalyst complexes under high H_2 pressure. Base, always added to promote turnovers in real catalyst systems by extracting formic acid from the catalyst, was not added to the reaction mixture in order to identify intermediate species by keeping the reaction at an equilibrium point. Furthermore, the backward step, that is reaction of formic acid with the catalyst, was studied and the whole reaction pathways could be connected. Effects of additives are not within the scope of this study. Several new aspects of the reaction intermediates and pathways are presented, and important criteria for designing better catalysts are suggested.

Results and Discussion

State of $[Ru(dmpe)_2H_2]$ in toluene: Figure 1 shows the IR spectrum of $[Ru(dmpe)_2H_2]$ in toluene at 300 K and calculated spectra of *cis*- and *trans*-$[RuH_2]$ complexes (from here on $(dmpe)_2$ is omitted). A broad Ru–H stretching band at

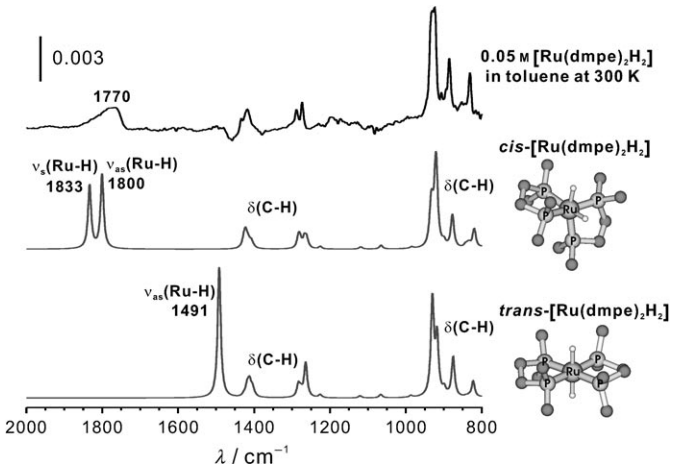

Figure 1. Comparisons between experimental and calculated IR spectra of $[Ru(dmpe)_2H_2]$. The optimized geometries are shown without hydrogen atoms of the dmpe ligands for clarity. Calculated vibrational frequencies are scaled by 0.97.

1770 cm^{-1} was observed, that is, the complex exists mostly in the *cis* form, as clearly seen from the calculated spectra. The good agreement for all the vibrational frequencies and intensities of the C–H bending and Ru–H stretching modes confirms the accuracy and reliability of the computational method and approximations applied. ^1H and ^{31}P NMR spectroscopy also show that the complex mainly exists as the *cis* isomer (Figure 2 for $^{31}P\{^1H\}$ and Supporting Information for ^1H). The peak at $\delta = 46.0$ ppm in the ^{31}P NMR spectrum was assigned to *trans*-[RuHCl], which is the intermediate before RuH_2 during synthesis from *trans*-$[RuCl_2]$. Although nearly all *trans*-$[RuCl_2]$ was converted to RuH_2 after synthesis, the residual NaCl in the solution reacted with the dihydride complex, and *trans*-[RuHCl] was formed (checked by means of the reaction between RuH_2 and NaCl). The concentration of *trans*-[RuHCl] was minor but gradually increased with time. Since most of the measurements reported here were carried out immediately after synthesis, except for high-pressure NMR spectroscopy, the presence of *trans*-[RuHCl] and the effects on the reaction pathway is neglected.

Octahedral ruthenium(II) dihydride complexes are known to be fluxional.[27] Field and co-workers reported that the *trans* isomer also exists at a ratio of *cis*:*trans* = 12:1 at 240 K in toluene.[28] We also confirmed the minor presence of the *trans* isomer based on ^{31}P and ^1H NMR data (quintet at $\delta = -10.3$ ppm in ^1H and $\delta = 49.0$ ppm in ^{31}P, see Supporting Information and reference [28]) and their 2D correlation. We obtained a ratio of *cis*:*trans* = 18:1 at 300 K in toluene.

State of $[Ru(dmpe)_2H_2]$ under CO_2 pressure and after addition of formic acid: Figure 2 shows the $^{31}P\{^1H\}$ NMR spectrum after the addition of 4 bar CO_2 to 0.03 M RuH_2 solution at 300 K. Immediately after addition, two Ru complexes, *cis*-$[Ru(OCHO)_2]$ and *trans*-[RuH(OCHO)], were observed as reported previously.[25] However, the expected intermediate *cis*-[RuH(OCHO)] before the formation of *cis*-[Ru-

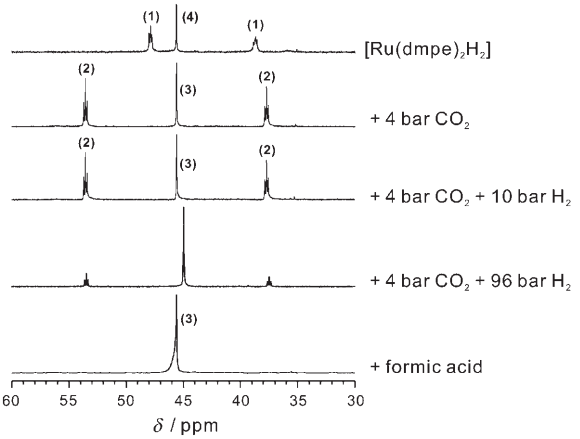

Figure 2. $^{31}P\{^1H\}$ NMR spectra of 0.03 M $[Ru(dmpe)_2H_2]$ in toluene at 300 K under different CO_2 and H_2 pressures or after addition of formic acid (molar ratio $[Ru(dmpe)_2H_2]$/formic acid = 1:2). 1) *cis*-$[Ru(dmpe)_2H_2]$, 2) *cis*-$[Ru(dmpe)_2(OCHO)_2]$, 3) *trans*-$[Ru(dmpe)_2H(OCHO)]$, and 4) *trans*-$Ru(dmpe)_2HCl$.

$(OCHO)_2]$ was not detected under the conditions applied, unlike the investigation at lower temperature and lower CO_2 pressure.[25] The ratio *trans*-[RuH(OCHO)]/*cis*-$[Ru(OCHO)_2]$ was significantly higher than *trans*-$[RuH_2]$/*cis*-$[RuH_2]$, and this suggests higher reactivity of *trans*-$[RuH_2]$ compared to *cis*-$[RuH_2]$ or higher stability of *trans*-[RuH(OCHO)] compared to *cis*-[RuH(OCHO)]. When the CO_2 pressure was released and the solution kept under Ar, the portion of *trans*-[RuH(OCHO)] increased with time with respect to *cis*-$[Ru(OCHO)_2]$, in agreement with the previous NMR study.[25] An interesting question is how the *trans*-[RuH(OCHO)] is formed, that is, by isomerization of formate complexes or by CO_2 insertion into *trans*-$[RuH_2]$. The feasibility of these pathways is discussed below.

Next, we investigated how formic acid interacts or reacts with RuH_2 at 300 K. After formic acid was added to the RuH_2 solution, H_2 was immediately formed and released as gas bubbles, and only *trans*-[RuH(OCHO)] was formed (Scheme 1). The assignment of *trans*-[RuH(OCHO)] was ensured by ^1H and ^{31}P NMR spectroscopy (Figure 2 and Supporting Information) and the doublet formate peak in the ^1H NMR spectrum after insertion of ^{13}C-enriched formic acid. Neither *cis*-[RuH(OCHO)] nor *cis*-$[Ru(OCHO)_2]$ was observed, although the hydride complex existed predominantly in the *cis* configuration prior to the reaction. Some

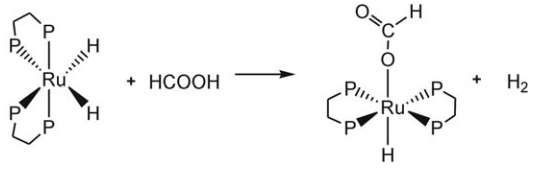

Scheme 1. Observed main reaction upon addition of formic acid to $[Ru(dmpe)_2H_2]$ in toluene at 300 K.

possible routes for the formation of *trans*-[RuH(OCHO)] were investigated in detail with the aid of DFT calculations (see below). The high reactivity of formic acid with RuH_2 and the formation of the formate complex (this step will be referred to as "formic acid reaction" or "substitution of hydride by formate") shed light on a very important aspect of the reaction system, that is, formed formic acid easily reacts with the hydride to form the formate complex during the hydrogenation of CO_2. This clearly shows the importance of removing formic acid from the vicinity of the hydride to avoid the backreaction and improve the catalytic performance.

The IR spectra of the Ru complexes formed after addition of CO_2 and formic acid are shown in Figure 3, as are the theoretical IR spectra of the formate complexes identified

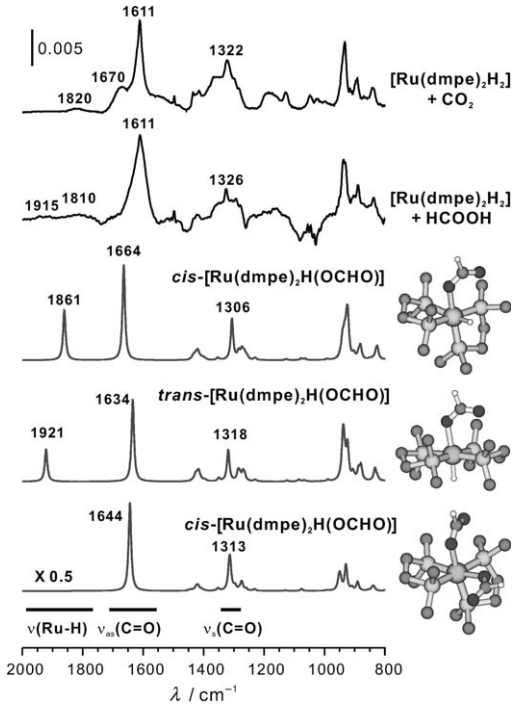

Figure 3. Top two spectra: Experimental IR spectra recorded after addition of 3 bar CO_2 or formic acid (molar ratio $[Ru(dmpe)_2H_2]$/formic acid = 1:2) to 0.05 M $[Ru(dmpe)_2H_2]$ in toluene at 300 K. Bottom three spectra: Calculated IR spectra of various formate complexes with the corresponding optimized geometries. For clarity hydrogen atoms of the dmpe ligands are not shown.

by NMR spectroscopy. Symmetric and asymmetric C=O stretching bands were observed at 1320–1330 and 1600–1700 cm^{-1}, respectively (formally, the formate group of the formate complexes contains one C=O bond and one C–O bond, but the length of the latter is close to that of the former, being greatly shorter than a typical C–O bond length. Therefore, the mode of the combined C=O and C–O stretching is denoted here simply as C=O stretching. The calculated IR spectra clearly show the presence of C=O stretching bands whose frequencies and intensities agree well with the experimental ones, and thus the assignment of

the vibrational modes is confirmed. However, the similar frequencies of the C=O stretching bands and the broad Ru–H stretching bands do not allow us to identify the formate complexes by IR spectroscopy alone. The main difference between the two experimental spectra in Figure 3 is the shoulder at 1670 cm^{-1}. The band most likely originates from *cis*-[Ru(OCHO)$_2$] because of its absence in the case of the reaction of formic acid with RuH_2. The rather broad band at 1670 cm^{-1} may originate from asymmetric C=O stretching vibrations averaged by different interactions of two formate groups.

State of [Ru(dmpe)$_2$H$_2$] under CO$_2$ and H$_2$ pressure: The state of the catalyst complex under H_2 and CO_2 pressure was investigated by high-pressure NMR and IR spectroscopy. After addition of 10 bar H_2 together with 4 bar CO_2, virtually no change was observed in the ^1H and ^{31}P NMR spectra (Figure 2 and Supporting Information) of the formate complexes compared to the spectra under CO_2 alone. However, when the H_2 pressure was increased to 96 bar, remarkable changes were observed in the ^1H and ^{31}P NMR spectra. More *trans* complex was formed and some shift to higher field was observed in ^1H and ^{31}P chemical shift. The hydride peak of the *trans* complex was nearly at the same chemical shift ($\delta = -22.9$ ppm) as that of *trans*-[RuH(OCHO)] ($\delta = -22.5$ ppm), but now appeared as a rather broad peak (see Supporting Information).

High-pressure IR investigations can often give helpful additional and complementary information due to the different timescale of IR compared to NMR spectroscopy. Figure 4 shows the high-pressure IR spectra of the complex under various pressures of CO_2 and H_2. First, 5 bar of CO_2 was added to the RuH_2 solution, and then H_2 was added and the pressure was gradually raised while keeping the CO_2 pressure at 5 bar. The total gas pressure was decreased when H_2 pressure reached 120 bar. Through the course of the experiments, large bands were observed in the regions of C–O, C=O, and Ru–H stretching vibrations. After complete release of the gas pressure, washing the ZnSe ATR crystal, and filling the IR cell with N_2, the measured IR spectrum clearly showed an accumulation of surface species on the crystal (Figure 4, marked with asterisks). The accumulation started above about 50 bar of H_2 pressure. This is most likely due to reaction between the surface of ZnSe and an Ru complex present under the high H_2 pressure. Generally, strong acids and bases react with ZnSe, so this suggests the formation of an acid- or baselike complex under high H_2 pressure. Interestingly, three bands at 1202, 1570, and 1725 cm^{-1} were present only under high H_2 pressure (>50 bar). These bands disappeared when the pressure was released. The three bands cannot be attributed to the formate complexes shown in Figure 3. The lack of the symmetric C=O stretching mode in the band pattern indicates that the C=O bond of the formate group is hydrogenated at high H_2 pressure. Due to the absence of base for extraction of formed formic acid from the catalyst, one of the most likely species existing under high H_2 pressure is that in which formic acid interacts with the hydride via an RuH_2···HOCHO dihydrogen bond. Figure 5 shows the structure and calculated IR spectra of

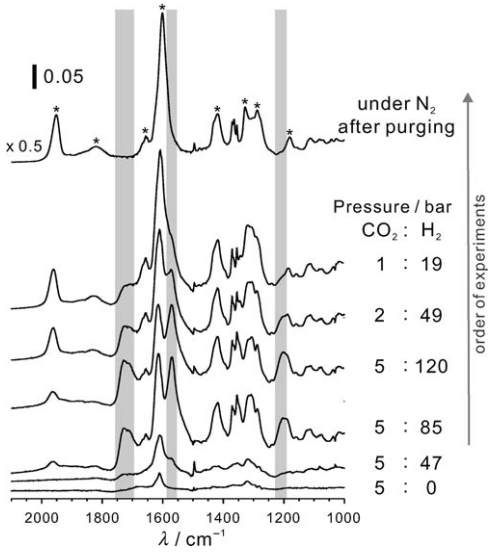

Figure 4. High-pressure IR spectra recorded after addition of CO_2 and H_2 to 0.05 M [Ru(dmpe)$_2$H$_2$] in toluene at 300 K. The bands which only appear under high H_2 pressure (>50 bar) are highlighted with gray shading. The spectrum of [Ru(dmpe)$_2$H$_2$] was taken as the background. The bands with asterisks are due to species that accumulated on the ZnSe ATR crystal during the measurements.

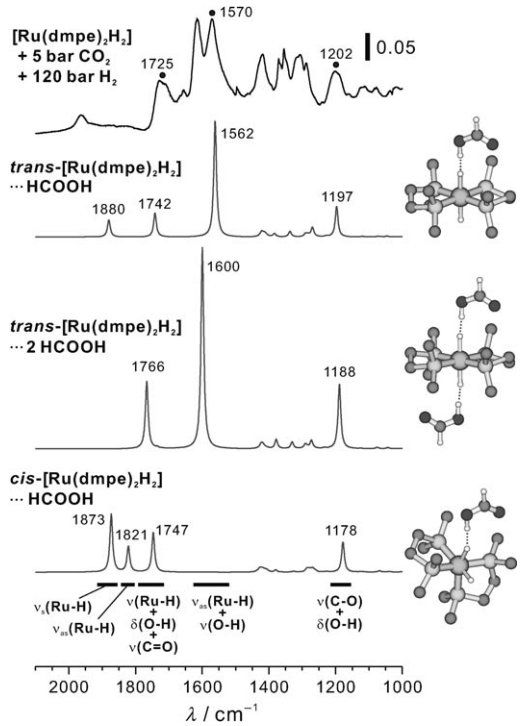

Figure 5. High-pressure IR spectrum recorded after the addition of 5 bar CO_2 and 120 bar H_2 to 0.05 M [Ru(dmpe)$_2$H$_2$] in toluene at 300 K and calculated IR spectra and optimized geometries of possible formed dihydrogen-bonded species. For clarity hydrogen atoms of the dmpe ligands are not shown. The bands marked with filled circles appeared only under high H_2 pressure (>50 bar) in the presence of a low CO_2 pressure (5 bar).

such complexes. *trans*-[RuH_2]···HOCHO clearly has the features of the species under high H_2 pressure and the agreement with the experimental spectrum is excellent. All the bands appearing under high H_2 pressure are combined with the bending or stretching mode of the OH group of formic acid. *trans*-[RuH_2]···2(HOCHO) also shows similar bands with slightly worse agreement with the experimental spectrum. The calculated spectrum of the *cis* analogue *cis*-[RuH_2]···HOCHO does not reproduce the large band near 1570 cm^{-1} observed in the experiment. The presence of dihydrogen bond was also confirmed by formation of the broad band at about 3200 cm^{-1} under high H_2 pressure, as reported before.[29] The similar chemical shift of the hydride peak of the high-pressure complex to that of *trans*-[RuH(OCHO)] (Supporting Information) suggests that the high-pressure species is likely *trans*-[RuH_2]···HOCHO. As seen previously, formic acid can easily react with the hydride complex and *trans*-[RuH(OCHO)] can then be formed. These observations clearly indicate that the reaction is highly reversible, and the equilibrium between the formate complex *trans*-[RuH(OCHO)] and the dihydrogen-bonded complex *trans*-[RuH_2]···HOCHO can be largely shifted to the latter under high H_2 pressure. The shorter timescale of IR spectroscopy is likely necessary to detect the dihydrogen-bonded complex at 300 K, probably due to the fast equilibrium. The experimentally observed reaction pathways are summarized in Scheme 2. The details of the pathways were investigated by DFT calculations (see below).

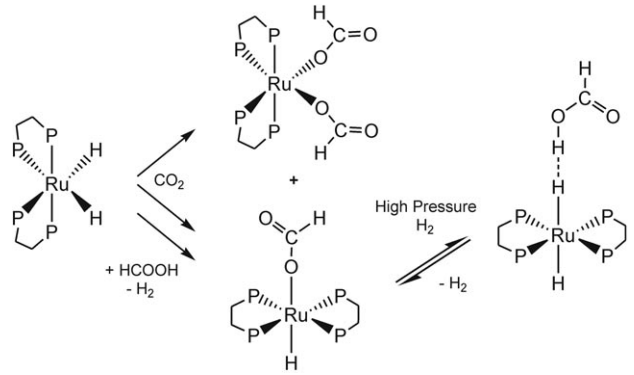

Scheme 2. Observed main reaction pathways of [$Ru(dmpe)_2H_2$] under CO_2 and H_2 pressure.

CO_2 insertion pathway: formation of *cis*-[$Ru(dmpe)_2H(OCHO)$] and *cis*-[$Ru(dmpe)_2(OCHO)_2$]: First, the formation pathways of the most abundant species under CO_2 pressure, *cis*-[$Ru(OCHO)_2$], and the most probable intermediate, *cis*-[RuH(OCHO)], were theoretically investigated (Figure 6). When CO_2 approaches a hydrido ligand of **1** (Ru–H 1.64 Å; important bond lengths and angles of the Ru complexes obtained by DFT calculations are given in the Supporting Information), it undergoes significant structural changes. Complex **2** resulting from the interaction between **1** and CO_2 has an RuH···C distance of 1.35 Å. In this study,

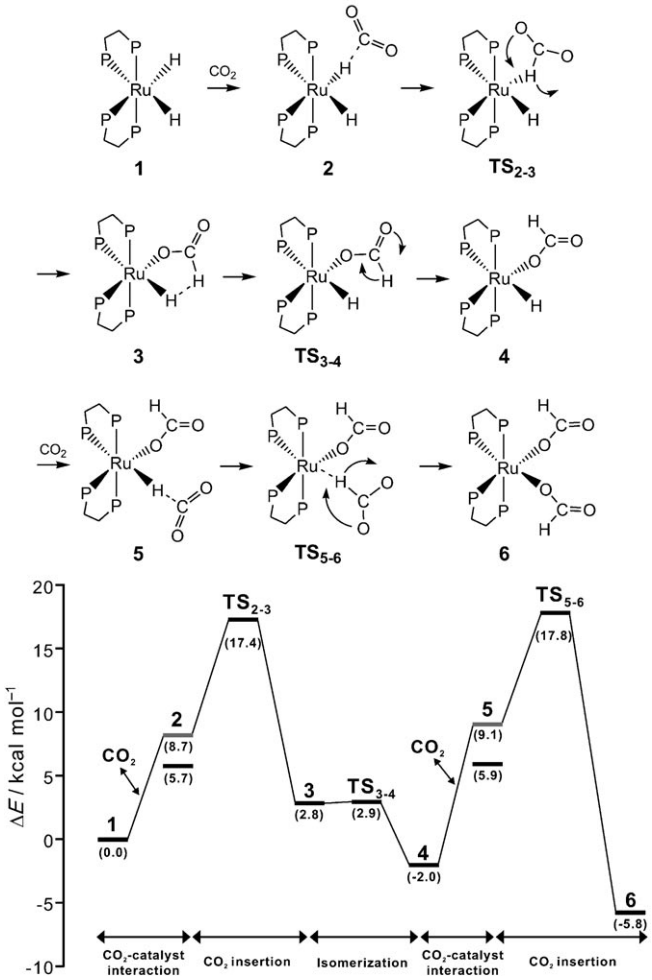

Figure 6. Potential-energy changes on CO_2 insertions during the formation of *cis*-[$Ru(dmpe)_2H(OCHO)$] and *cis*-[$Ru(dmpe)_2(OCHO)_2$]. Corrections for zero-point vibrational energies were made. BSSE-corrected energies of complexes with CO_2–hydride interaction are shown by a gray bar.

such complexes in which CO_2 interacts with a hydrido ligand are considered to be the initial step of the CO_2 insertion process. The C=O bond of CO_2 (C=O 1.16 Å) and the Ru–H bond of **2** interacting with CO_2, are slightly elongated (1.21 and 1.76 Å, respectively) and the OCO angle is reduced significantly, by 38°.

The coordination of an oxygen atom to the Ru center and the formation of formate complex **3** occur via **TS_{2-3}** (337 *i* cm^{-1}) by means of two concerted events: Ru–H bond breaking and O coordination, with an activation energy of 8.7 kcal mol^{-1} (11.7 kcal mol^{-1} without BSSE correction). The concerted insertion mechanism is different from the previously reported concerted mechanisms in that there is no initial interaction of an O atom with or coordination of an O atom to the metal center.[20–22,30] This relatively small activation energy is in good agreement with the facile CO_2 insertion observed experimentally. Ab initio metadynamics studies also confirmed very facile insertion of CO_2 into RuH_2 complexes with the same concerted insertion mecha-

nism.[31] The Ru–H bond of $\mathbf{TS_{2\text{-}3}}$ is elongated to 2.30 Å and the Ru···O distance is 2.92 Å. Interestingly, the formate unit of $\mathbf{TS_{2\text{-}3}}$ undergoing rotational movement has nearly the same bond lengths and angles as the formate ion $COOH^-$ (for details, see Supporting Information). The C–H and C=O bond lengths and OCO angle of $\mathbf{TS_{2\text{-}3}}$ are 1.15 (C–H), 1.26 (C=O, close to the Ru center), 1.23 Å (C=O, remote from the Ru center), and 130° (O-C-O), while the values for the formate ion are 1.16 (C–H), 1.25 Å (C=O), and 131° (O-C-O). The insertion can be regarded as rotation of the formate ion near the RuH^+ ion at the transition state $\mathbf{TS_{2\text{-}3}}$. The character of the formate group and the bonding is investigated in more detail below.

Complex **3**, in which the hydrogen atom of the formate group weakly interacts with the hydrido ligand (H···H 2.45 Å), is formed after the transition state. The C–O bond length involving the O atom coordinated to the Ru center is elongated to 1.30 Å, while the noncoordinating C=O bond length is 1.22 Å. Formate complex **3** is not the most stable *cis*-[RuH(OCHO)] species. The formate group of **3** rotates via $\mathbf{TS_{3\text{-}4}}$ ($131\,i\,cm^{-1}$) with a very small energetic barrier ($0.1\,kcal\,mol^{-1}$) to give **4**, in which the formate hydrogen atom points away from the Ru center and the formate oxygen atom is in the vicinity of the methyl hydrogen atoms of the dmpe ligand. The energetic stability of this isomer relative to the others was assured by scanning a dihedral angle, that is, a series of geometry optimizations of stereoisomers with different P-Ru-O-C dihedral angles. Formate complex **4** is $2.0\,kcal\,mol^{-1}$ more stable than dihydride complex **1**. The C–O bond of **4** is slightly shortened to 1.28 Å, while the C=O distance is elongated to 1.23 Å with respect to **3**. As shown before, mono-formate complex *cis*-[RuH(OCHO)] (**4**) was not observed experimentally, and instead only bis-formate complex *cis*-[Ru(OCHO)$_2$] (**6**) was detected.

The second CO_2 insertion occurs via an identical pathway to the first. First, close interaction of CO_2 with hydride complex **5** results in significant CO_2 deformation, that is, longer C=O bonds (1.20 Å) and bent OCO angle (145°). Through a similar transition state $\mathbf{TS_{5\text{-}6}}$ ($313\,i\,cm^{-1}$) to the first CO_2 insertion via the concerted mechanism, bis-formate complex **6** is formed. The energetic profile is also similar to that of the first CO_2 insertion. The same activation energy of $8.7\,kcal\,mol^{-1}$ for the insertion is obtained, and this implies that the second CO_2 insertion will occur after the first when enough CO_2 molecules are in the vicinity of the hydride complex to form complex **2** or **5** with the CO_2–hydride interaction. Bis-formate complex **6** is $5.8\,kcal\,mol^{-1}$ more stable than dihydride complex **1**, and this agrees with the stability of **6** observed experimentally.

CO_2 insertion pathway: formation of *trans*-[Ru(dmpe)$_2$H(OCHO)]: When 4–5 bar CO_2 pressure was applied to the catalyst solution, mono-formate complex *trans*-[RuH(OCHO)] was also observed in addition to **6**. The amount of this complex was less than that of **6** under this CO_2 pressure; however, it was formed instantaneously and the concentration gradually increased with time when the CO_2 pressure was released. Here the formation mechanism of *trans*-mono-formate complex **9** is investigated (Figure 7).

There are several possibilities for forming **9** starting from dihydride complex **1**. One possible route is via isomerization

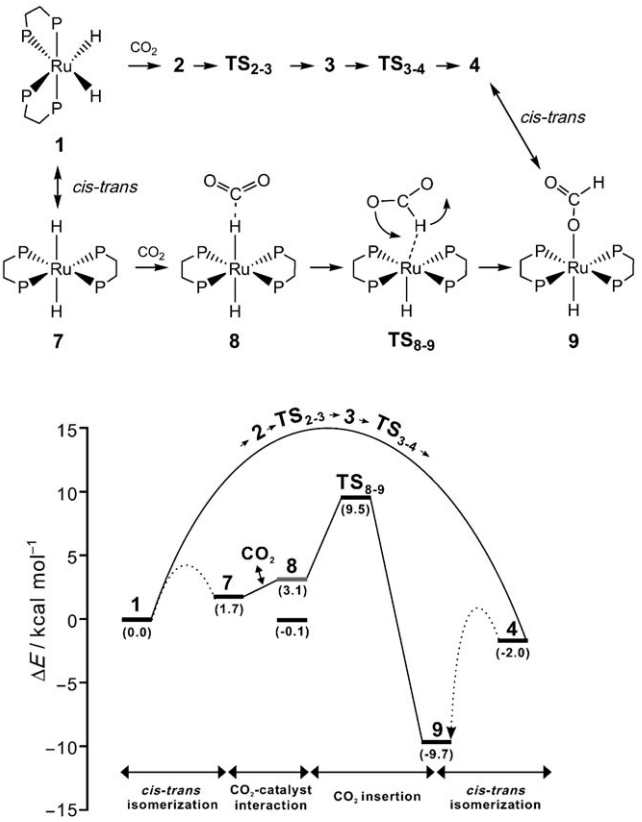

Figure 7. Potential-energy changes on CO_2 insertion during the formation of *trans*-[Ru(dmpe)$_2$H(OCHO)] with isomerization possibilities (shown as dotted lines, required activation energy is arbitrary). Corrections for zero-point vibrational energies were made. BSSE-corrected energy of complex with CO_2–hydride interaction is shown by a gray bar.

of mono-formate *cis* complex **4** (Figure 7). This route is nearly impossible to analyze by using static models; therefore, we studied the pathway by ab initio metadynamics, which indicated that formation of **9** via **4** is possible but unlikely.[31] Another possible route is via *trans*-[RuH_2] (**7**). As shown before, **7** is in equilibrium with **1** and exists in a small fraction. Previous NMR studies indicated that the CO_2 insertion/dissociation step between **1** and **4** is likely reversible,[25] that is, the pathway **4**→**1**→**7** is possible. Taking account of the previously suggested higher reactivity of the *trans* dihydride **7** relative to *cis* isomer **1** for CO_2 insertion, the *cis–trans* equilibrium can shift towards *trans* after CO_2 insertion. Additionally, the higher stability of *trans* formate complex **9** (Figure 7) compared to *cis* formate complex **4** can be the source of the equilibrium shift towards *trans* when the CO_2 insertion/dissociation process is reversible and *cis* (**1**) and *trans* (**7**) hydrido complexes are in equilibrium. The maximum rate of *cis–trans* isomerization at 323 K has been reported to be at most $0.1\,s^{-1}$,[28] which supports

slow, but finally dominant, formation of *trans* formate complex **9**.

After CO_2 dissociation from **4**, CO_2 insertion (Figure 7) occurs via a route analogous to CO_2 insertion into *cis* complexes **1** and **4** (Figure 6). First, CO_2 approaches and interacts with **7**, and this results in deformation of CO_2. The C=O bonds are elongated to 1.22 Å, and the O-C-O angle is strongly bent to 139°, that is, greater deformation than in the case of the *cis* complexes. The RuH···C distance of 1.26 Å is shorter than those in the *cis* cases (**2**, **5**). Energetically the CO_2–hydride interaction complex is formed more easily for the *trans* complex (1.4 kcal mol^{-1}) than the *cis* complexes (8.7–11.1 kcal mol^{-1}), probably due to less steric hindrance when CO_2 approaches the hydrido ligand. In addition, the slightly longer Ru–H bond (1.69 Å) of **7** compared to that of *cis* complex **1** (1.64 Å) may facilitate the interaction of CO_2 in the vicinity of the Ru center.

The CO_2 insertion occurs by a concerted insertion mechanism similar to that shown for the *cis* cases in Figure 6 with a transition state $\mathbf{TS_{8\text{-}9}}$ (301 i cm^{-1}). The vibrational mode corresponding to the imaginary eigenfrequency is similar to those of $\mathbf{TS_{2\text{-}3}}$ and $\mathbf{TS_{5\text{-}6}}$, while the formate group rotating near the Ru center shows bond lengths (C=O 1.23, 1.26 Å; C–H 1.15 Å) and angle (O-C-O 131°) that are even closer to those of the formate ion (C=O 1.25, C–H 1.16 Å; O-C-O 131°) than in the *cis* cases ($\mathbf{TS_{2\text{-}3}}$ and $\mathbf{TS_{5\text{-}6}}$). After $\mathbf{TS_{8\text{-}9}}$, stable mono-formate *trans* complex **9** is formed, which is more stable (9.7 kcal mol^{-1} with respect to **1**) than the *cis* formate complexes (**4** and **6**). A lower activation energy (6.4 kcal mol^{-1}) than for the *cis* cases (8.7 kcal mol^{-1}) is found. When the easier CO_2 interaction and the lower barrier are considered, faster formation of *trans* formate complex **9** can be expected relative to *cis* formate complexes **4** and **6**. This confirms the higher reactivity for CO_2 insertion via the *trans* route. The stability of **9** is also in agreement with the experimental observations, that is, **9** is the most abundant species in solution after a long time without CO_2 pressure.

The formation of **9** can also occur from **6** via 1) *cis–trans* isomerization of **6** and then dissociation of CO_2, 2) dissociation of CO_2 from **6** and *cis-trans* isomerization of **4**, and/or 3) CO_2 dissociation from **6** to give **1**, *cis–trans* isomerization from **1** to **7**, and CO_2 insertion. Based on the ab initio metadynamics study,[31] the most likely pathway is 3). The gradual change in concentration from **6** to **9** is probably due to the high energy barriers for CO_2 dissociation from **6** (19.4 kcal mol^{-1}) and **4** (23.6 kcal mol^{-1}), as well as the relatively slow isomerization between **1** and **7**.

Pathway of formic acid formation from *trans*-[Ru(dmpe)$_2$H(OCHO)]: Since the discovery of a high turnover frequency of formic acid formation with Ru catalysts in supercritical CO_2, strong dependence of the reaction rate on H_2 pressure has been reported.[12,15,23,24] It was already noted that the high solubility of H_2 in supercritical CO_2 is the most likely origin of the high reaction rate.[15] These observations imply that the reaction between H_2 and the formate complex is the rate-limiting step, although some theoretical studies concluded the CO_2 insertion is rate-limiting.[20,21] This work and previous NMR studies[25] on [Ru(dmpe)$_2$H$_2$] clearly show facile insertion of CO_2 and facile formation of formate complexes, so CO_2 insertion is not likely to be the rate-limiting step. In the high-pressure IR and NMR investigations, the intermediate before the product, that is formic acid interacting with the hydride catalyst, could only be detected at high H_2 pressure (Figure 5), and the intermediate concentration strongly depended on H_2 pressure (Figure 4). This experimental observation implied that the H_2 insertion step to form the formate complex requires greater activation than CO_2 insertion, and therefore high H_2 pressure is required to shift the equilibrium (Scheme 2). The H_2 insertion to form formate complex **9** was theoretically investigated.

Thorough search for the transition state with the help of ab initio metadynamics[31] found H_2-insertion transition state $\mathbf{TS_{9\text{-}10}}$ (277 i cm^{-1}, Figure 8), in which a hydrogen molecule

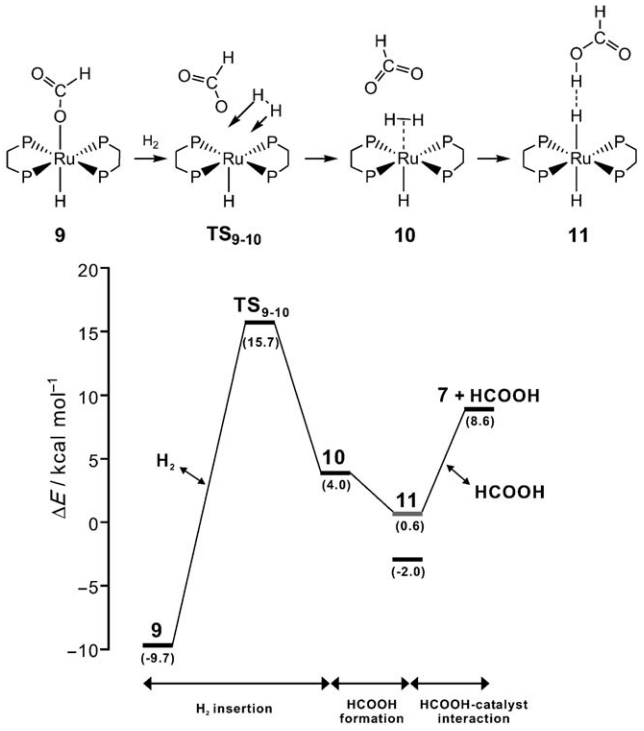

Figure 8. Potential-energy changes on H_2 insertion into *trans*-[Ru(dmpe)$_2$H(OCHO)]. Corrections for zero-point vibrational energies were made. BSSE-corrected energy of dihydrogen-bonded complex is shown by a gray bar.

approaches the Ru center (Ru···H_2 ca. 2.5 Å) with a slightly elongated H–H bond (0.77 Å, isolated H_2: 0.75 Å). Such a notable ligand displacement by molecular hydrogen is similar to those reported for Cl[32] and other ligands.[33] The Ru–O bond is remarkably elongated to 3.10 from 2.28 Å. The activation energy for $\mathbf{TS_{9\text{-}10}}$ is four times higher (25.4 kcal mol^{-1}) than in the case of CO_2 insertion (6.4 kcal mol^{-1}). From the bond lengths of the transition state, it is likely that the high energy of $\mathbf{TS_{9\text{-}10}}$ is due to the long Ru–O bond and

the remoteness of the formate group from the Ru center. A more detailed analysis of the bond characteristics is given below.

After H_2 insertion, experimentally observed H···H dihydrogen-bonded complex **11** is formed via Ru(η^2-H_2) complex **10**, in which molecular H_2 is coordinated to the Ru center. Such η^2-H_2 complexes, for example, found by Kubas,[34,35] have been increasingly reported, and the role of such complexes in catalytic hydrogenation is an interesting branch of fundamental research. The H–H distance of **10** of 0.85 Å belongs to the category of "true H_2 complexes" by the definition of Kubas.[35] The existence of **10** and the relative stability are suggested by ab initio metadynamics when both H_2 and formic acid concentrations are sufficiently high.[31] The bond characteristics of the formate part of **10** are not different from those of **9** and $\mathbf{TS_{9\text{-}10}}$. The interesting Ru($\eta^2$-$H_2$) complex **10** consists of two parts, *trans*-[RuH(η^2-H_2)]$^+$ and formate ion, and **10** can be regarded as the interaction of these two ions (in this work, the whole structure including the formate group is regarded as a complex, and we therefore denote the complex by the neutral Ru(η^2-H_2) notation unless the ionic parts are explicitly and separately considered). The Ru(η^2-H_2) complex **10** was not observed in the experiments, likely due to the existence of the more stable dihydrogen-bonded complex **11**.

When one hydrogen atom of the η^2-H_2 ligand of **10** interacts with a formate oxygen atom, the dihydrogen-bonded complex **11** is formed. No transition state could be found between **10** and **11**. The dihydrogen-bond strength of **11** is 8.0 kcal mol^{-1} (BSSE considered) and the binding is very strong for a hydrogen bond. This strong dihydrogen bond suggests that the backreaction, that is, reaction of formic acid with RuH_2, can easily take place, and therefore the extraction of formic acid from the catalyst, typically done by addition of an organic base, must be well engineered. Indeed, the choice of base significantly affects the catalytic performance.[15,36]

Pathway of formic acid reaction with [Ru(dmpe)$_2$H$_2$]: The facile reaction of formic acid with the hydride complex and the rapid formation of *trans*-formate complex **9** and gaseous H_2 were observed experimentally. Only *trans*-formate complex **9** and no *cis*-formate complex **4** were detected after the reaction. There are three possibilities for the reaction path: 1) reaction of formic acid with *trans*-[RuH_2], 2) reaction of formic acid with *cis*-[RuH_2] to form *cis*-[RuH(OCHO)] followed by *cis–trans* isomerization, and 3) reaction of *cis*-[RuH_2] with formic acid giving H_2 and $RuH^+\cdots OCHO^-$ followed by the *cis–trans* isomerization of RuH^+.

The first route is equivalent to the backward pathway shown in Figure 8. The strong dihydrogen-bonding interaction of **11** may facilitate this process. The activation energy for the substitution process of hydride by formate is 15.1 kcal mol^{-1}. In toluene, formic acid is likely to interact with polar molecules due to the apolar character of toluene; therefore, the probability of the dihydrogen-bonding interaction is further enhanced.

The second possible pathway of formic acid reaction is via the *cis* route. The energetic profile is shown in Figure 9. The dihydrogen-bonding interaction in complex **12** is strong

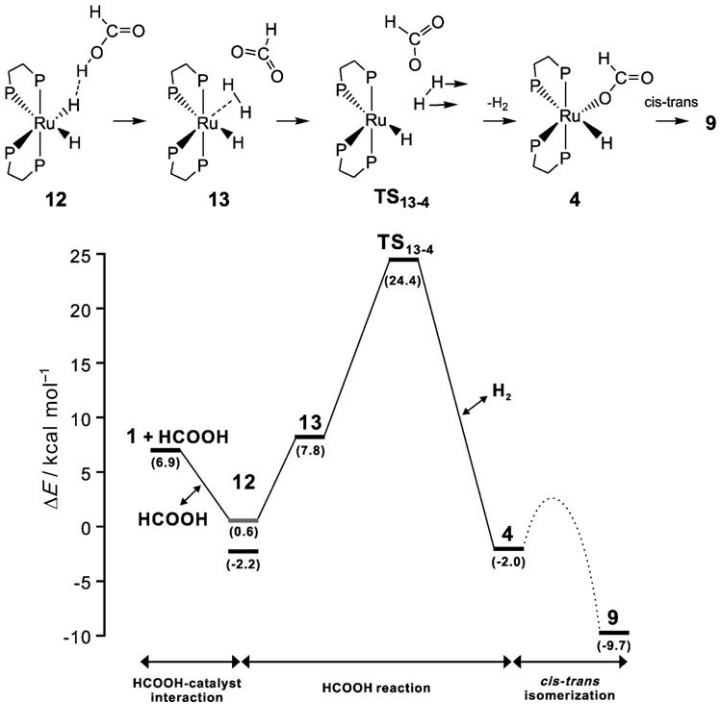

Figure 9. Potential energy changes on reaction of formic acid with *cis*-[Ru(dmpe)$_2$H$_2$] to form [Ru(dmpe)$_2$H(OCHO)] formate complexes. Corrections for zero-point vibrational energies were made. BSSE-corrected energy of dihydrogen-bonded complex is shown by a gray bar.

(6.3 kcal mol^{-1}) with an H···H distance of 1.65 Å, but weaker than that of *trans*-[RuH_2]···H(OCHO) (**11**). The reaction of formic acid with RuH_2 occurs through a similar pathway as in the *trans* case, that is, via η^2-H_2 complex **13**. The *cis*-[RuH(η^2-H_2)]···OCHO complex **13** has three hydrogen atoms coordinated to the Ru center next to each other. The two hydrogen atoms that coordinate after insertion of molecular H_2 interact at an H···H distance of 0.89 Å, which also belongs to the group of "true H_2 complexes".[35] The formate part, which apparently interacts as "formate ion" with *cis*-[RuH(η_2-H_2)]$^+$, shows bond character that resembles formate ion more than formic acid (see below and Supporting Information for details). The two molecularly coordinating hydrogen atoms of RuH(η_2-H_2)$^+$ dissociate from the Ru center as molecular hydrogen, and formate complex **4** is formed via transition state $\mathbf{TS_{13\text{-}4}}$ with an activation energy of 23.8 (26.6) kcal mol^{-1} (energy without BSSE correction in parentheses, and **12** was considered as the initial state), which is 8.7 kcal mol^{-1} higher than that obtained for the *trans* route (Figure 8). This is mainly due to the higher energy of the transition state of the *cis* form compared to the *trans* form. Similar to $\mathbf{TS_{9\text{-}10}}$, the Ru···O distance is significantly elongated to 3.2 Å, slightly longer than in $\mathbf{TS_{9\text{-}10}}$

(3.1 Å). The Ru···H_2 distance is about 2.4 Å, slightly shorter than in the *trans* case (ca. 2.5 Å). The lower activation energy and stronger dihydrogen bond of the *trans* route can result in faster reaction than for the *cis* route, which can explain the preferential formation of *trans* formate complex **9**.

The third possible pathway involves isomerization of RuH^+ after $\mathbf{TS_{13\text{-}4}}$ in Figure 9. The five-coordinate RuH^+ complex is considered to be highly fluxional, and *cis* to *trans* isomerization may proceed, partly assisted by the stability of the *trans* isomer.[28] However, such a RuH^+ complex has been identified only in polar media,[28] and the pathway would be possible only when RuH^+ and formate ions are well stabilized. In apolar media like toluene, as used in this study, formation of stabilized ions is unlikely.

Considering the three possible routes for the formation of *trans*-[RuH(OCHO)], the most probable pathway is the first one. The second route may occur simultaneously due to the low stability of *cis*-[RuH(OCHO)], as observed experimentally.[25]

Characteristics of Ru complexes: The previous sections showed the differences between *cis* and *trans* routes, the "formate ion" interaction model, and the presence of interesting intermediate Ru(η_2-H_2) complexes. Characteristics of the bonds and the interactions are further discussed in this section on the basis of NBO analysis.[37]

Table 1 lists the natural charges and valence natural electron configurations of selected compounds relevant to this work. Expected complexes during formic acid formation via *cis* and *trans* mono-formate routes are shown. So far, only the *trans* route has been considered for H_2 insertion into the mono-formate complex (Figure 8). A comparable H_2 insertion pathway via the *cis* route can also be obtained from the reverse pathway of the reaction of formic acid with RuH_2 via the *cis* route (Figure 9). Table 1 compares the equivalent *cis*- and *trans*-[Ru] complexes on the reaction paths. There are several differences between the *cis* and *trans* routes.

First, the natural charges of Ru fluctuate more significantly on the *cis* route. The natural charges of Ru in dihydride complexes **1** and **7** and dihydrogen-bonded complexes **12** and **11** are similar, but Ru becomes more positively (less

Table 1. Natural charges and valence natural electron configurations of selected molecules and complexes. The p-orbital occupancy of Ru and d-orbital occupancy of C and O are not shown due to the negligible contributions. H(1)/H(2) and H(3)/H(4) originate from the dihydride complex and molecular H_2, respectively. H(1) results in the formate hydrogen atom (C–H) and H(3) results in the OH hydrogen of formic acid. O(1) is the oxygen which coordinates to the Ru center and reacts with H(3).

	Ru	H(1)	H(2)	H(3)	H(4)	C	O(1)	O(2)
CO_2						0.992 $s^{0.65}p^{2.31}$	−0.496 $s^{1.72}p^{4.76}$	−0.496 $s^{1.72}p^{4.76}$
H_2				0.000	0.000			
formic acid		0.115		0.478		0.651 $s^{0.86}p^{2.44}$	−0.675 $s^{1.69}p^{4.97}$	−0.569 $s^{1.72}p^{4.76}$
formate ion		−0.057				0.617 $s^{0.82}p^{2.50}$	−0.780 $s^{1.73}p^{5.04}$	−0.780 $s^{1.73}p^{5.04}$
cis-[RuH_2] (**1**)	−0.996 $s^{0.41}d^{8.56}$	−0.102	−0.102					
cis-[RuH_2]···CO_2 (**2**)	−0.843 $s^{0.38}d^{8.43}$	−0.059	−0.084			0.816 $s^{0.72}p^{2.40}$	−0.654 $s^{1.71}p^{4.93}$	−0.641 $s^{1.71}p^{4.92}$
cis-[RuH_2]···CO_2 ($\mathbf{TS_{2\text{-}3}}$)	−0.711 $s^{0.37}d^{8.32}$	0.072	−0.086			0.613 $s^{0.82}p^{2.50}$	−0.768 $s^{1.73}p^{5.03}$	−0.712 $s^{1.71}p^{4.99}$
cis-[RuH(OCHO)] (**4**)	−0.670 $s^{0.37}d^{8.27}$	0.077	−0.083			0.666 $s^{0.82}p^{2.46}$	−0.733 $s^{1.69}p^{5.02}$	−0.704 $s^{1.72}p^{4.98}$
cis-[RuH(OCHO)]···H_2 ($\mathbf{TS_{13\text{-}4}}$)	−0.658 $s^{0.35}d^{8.28}$	0.058	−0.093	0.048	−0.023	0.645 $s^{0.83}p^{2.46}$	−0.802 $s^{1.73}p^{5.06}$	−0.753 $s^{1.72}p^{5.02}$
cis-[RuH(η^2-H_2)(OCHO)] (**13**)	−0.903 $s^{0.39}d^{8.49}$	0.056	−0.074	0.177	0.073	0.647 $s^{0.83}p^{2.46}$	−0.799 $s^{1.73}p^{5.06}$	−0.750 $s^{1.72}p^{5.02}$
cis-[RuH_2]···HOCHO (**12**)	−0.956 $s^{0.40}d^{8.53}$	0.103	−0.087	0.496	−0.178	0.664 $s^{0.85}p^{2.44}$	−0.729 $s^{1.68}p^{5.04}$	−0.606 $s^{1.71}p^{4.88}$
trans-[RuH_2] (**7**)	−0.992 $s^{0.42}d^{8.55}$	−0.220	−0.220					
trans-[RuH_2]···CO_2 (**8**)	−0.881 $s^{0.40}d^{8.46}$	−0.073	−0.038			0.768 $s^{0.74}p^{2.43}$	−0.680 $s^{1.72}p^{4.95}$	−0.681 $s^{1.72}p^{4.95}$
trans-[RuH_2]···CO_2 ($\mathbf{TS_{8\text{-}9}}$)	−0.787 $s^{0.38}d^{8.38}$	0.030	0.036			0.626 $s^{0.81}p^{2.50}$	−0.773 $s^{1.73}p^{5.04}$	−0.707 $s^{1.71}p^{4.98}$
trans-[RuH(OCHO)] (**9**)	−0.738 $s^{0.37}d^{8.34}$	0.070	−0.068			0.659 $s^{0.82}p^{2.46}$	−0.743 $s^{1.70}p^{5.02}$	−0.733 $s^{1.72}p^{5.00}$
trans-[RuH(OCHO)]···H_2 ($\mathbf{TS_{9\text{-}10}}$)	−0.727 $s^{0.36}d^{8.34}$	0.050	0.043	0.105	−0.114	0.642 $s^{0.83}p^{2.47}$	−0.812 $s^{1.73}p^{5.07}$	−0.730 $s^{1.72}p^{5.00}$
trans-[RuH(η^2-H_2)(OCHO)] (**10**)	−0.934 $s^{0.39}d^{8.50}$	0.046	−0.064	0.133	0.032	0.641 $s^{0.83}p^{2.46}$	−0.822 $s^{1.73}p^{5.08}$	−0.743 $s^{1.72}p^{5.01}$
trans-[RuH_2]···HOCHO (**11**)	−0.951 $s^{0.40}d^{8.52}$	0.099	−0.166	0.483	−0.299	0.664 $s^{0.84}p^{2.44}$	−0.717 $s^{1.68}p^{5.03}$	−0.625 $s^{1.71}p^{4.90}$

negatively) charged during the reaction via the *cis* route. Also, the natural charges of the hydrogen atom that is not involved in the reaction and remains as a hydride (H(2) in Table 1), are nearly constant for the *cis* complexes, while those of the *trans* complexes vary from negative to positive. The positive charges are found at the transition states (**$TS_{8\text{-}9}$** and **$TS_{9\text{-}10}$**). Before CO_2 insertion (**7** to **$TS_{8\text{-}9}$**), the charge of hydride H(2) on the *trans* route seemingly changes in accordance with the other hydride H(1), which is interacting and reacting with CO_2. One possible reason for the lower charge fluctuation of Ru in *trans* complexes and for the higher fluctuation of the hydride charge is that the electrons of the hydride can be transferred and donated to Ru. Judging from the net charge of CO_2 of **8**, roughly 0.6 e must be transferred from the Ru complex to the CO_2 already in the initial stage of CO_2 insertion. The NBO analysis showed that, interestingly, there is formally no σ(Ru–H) bond in **7**; instead σ(H–H) and σ*(H–H) exist with occupancies of 0.689 and 1.743, respectively. Commonly, Ru complexes have three lone pairs, but four lone pairs on Ru were identified, three with 100% d character and high occupancy (ca. 1.9) and one with a slight p character (3.7%) and an occupancy of 1.505. The fourth lone pair is unique and only exists in **7** among the complexes of the current study. Furthermore, donor–acceptor analysis by second-order perturbation theory[38] showed an extraordinary large energetic stabilization (334.5 kcal mol^{-1}) due to n(Ru)→σ(H–H) interaction (Figure 10 a). In Figure 10, pre-orthogonal natural bond orbitals (PNBOs) are shown because overlap of the orbitals signifies energy stabilization by the corresponding interactions.[38] The n(Ru)→σ(H–H) interaction is responsible for the high degree of electron delocalization of the complex, and therefore the hydrido ligands can transfer the electrons mutually through Ru. This unique character of the *trans* dihydride complex **7** can explain the charge-fluctuations trends of Ru and H, as well as the apparent synchronized charges of the hydrido ligands in the *trans* complexes.

In the above DFT investigations, the formate part of the complexes during the course of the reaction paths resembles the geometry of the formate ion. The natural charges and especially the electron configurations of C and O clearly support these conclusions. In the initial CO_2 interaction step (**2**, **8**), the hybridizations of C and O lie between those of CO_2 and formate ion. However, after the step (**2**, **8**) until formic acid formation (**12**, **11**) the hybridizations are very close to those of formate ion. There is one considerable difference between the *cis* and *trans* routes. The charges of C and O of *trans* complex **8** are more negative than those of *cis* complex **2** during the initial interaction step. This could be due to the more negative hydride charge on the *trans* hydrides and also the weaker Ru–H bonding, indicated by the longer bond (*cis*: 1.64 Å, *trans*: 1.69 Å), which facilitates electron transfer via the *trans* route. Indeed, the NBO analysis clearly shows significant electron transfer during the interactions. The NBO of Ru–H of **8** in which H is interacting with CO_2 is 0.145, while the RuH···C bond order of 0.722 shows stronger bonding of the latter. For the *cis* equivalent

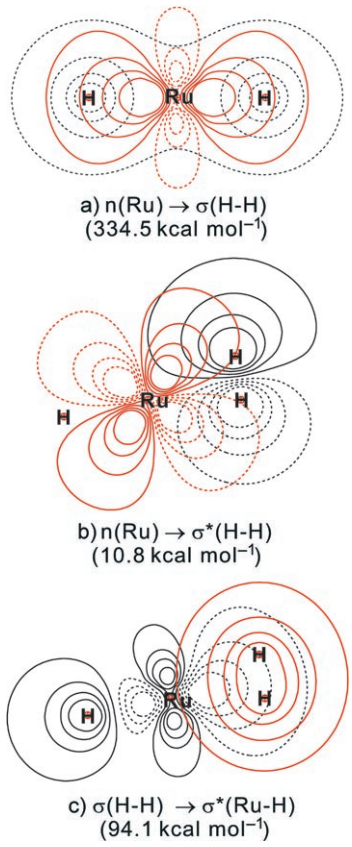

Figure 10. Major donor (red contours)–acceptor (black contours) interactions of Ru complexes **7** and **10**. a) n(Ru)→σ(H–H) interaction of **7**. b) n(Ru)→σ*(H–H) interaction and c) σ(H–H)→σ*(Ru–H) interaction of **10**.

2, 0.280 (Ru–H) and 0.616 (RuH···C) are found. These remarkable changes in bond order indicate that the bonding, more precisely the electron distribution, is significantly different when CO_2 interacts very closely with the hydrido ligands of the isolated dihydride complex **7** (and **1**) and CO_2. The electrostatic potential of **8** is shown in Figure 11. It clearly shows more shared electron density between the hydride and C than the hydride and Ru, proof that already in the initial step, CO_2 interaction in the vicinity of the hydride complexes significantly changes the character of the chemical bonding. In particular, the change is more pronounced on the *trans* route. Hereafter, only the lower energy *trans* route is further investigated.

After the CO_2–dihydride interaction (**8**), formate complex **9** is formed via transitions state **$TS_{8\text{-}9}$**. The electrostatic potential plot of **$TS_{8\text{-}9}$** in Figure 11 shows no density at the chosen density isosurface (0.06 a.u.) and very low bond orders (Ru–H: 0.038, Ru–O: 0.003, see Supporting Information) in addition to the similar hybridizations of C and O as in formate ion (Table 1), in support of the previously suggested view of "rotating formate ion". Surprisingly, the bond order of the Ru–O bond of formate complex **9** formed after **$TS_{8\text{-}9}$** is also very low (0.066) and no Ru–O bond was assigned by the NBO analysis. The electrostatic potential plot

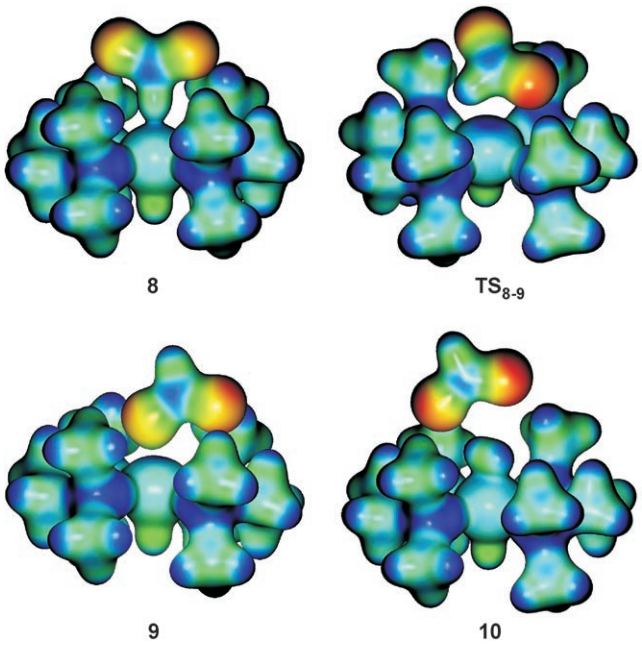

Figure 11. Electrostatic potentials plotted on the isosurface of electron density (0.06 a.u.) of selected Ru complexes. Color code: red < -0.08, yellow 0.00, green 0.10, light blue 0.20, and blue > 0.40 a.u.

(Figure 11) clearly shows no shared electron above the chosen density threshold (0.06 a.u.) and highly localized electrons, and this implies highly ionic character of the Ru–O bond.

Via the H_2-insertion transition state **TS_{9-10}** after **9**, the interesting complex *trans*-[RuH(η^2-H_2)]···OCHO (**10**) is formed. Members of this class of molecular η^2-H_2 complexes have been increasingly reported[34,35,39] and often suggested as intermediates during hydrogenation[40,41] and hydrogenolysis.[42,43] Dihydrogen bonding is also frequently reported for η^2-H_2 complexes as intermediates or as stable complexes,[44] depending on the proton-donor capacity.[45,46] The pathway of H_2 insertion or reaction of formic acid with RuH_2 described in Figure 8 lies in the same category. The origins of the complex stability were analyzed by donor–acceptor interactions. Considerable interactions between Ru and H_2 (10.8 kcal mol^{-1}, n(Ru)→σ*(H–H), Figure 10b) and between H_2 and the Ru–H bond (94.1 kcal mol^{-1}, σ(H–H)→(σ*(Ru–H), Figure 10c) are found in addition to more "dative" interactions from H_2 to the Rydberg orbital of Ru (σ(H–H)→n*(Ru), total 40.8 kcal mol^{-1}). Therefore, the bonding character of **10** between Ru and molecular hydrogen can be understood as "synergistic H_2 coordination" due to the donating/backdonating interactions,[38] and the stability of the complex can be attributed to these interactions. The formate ion part of **10** has little interaction with the *trans*-[RuH(η^2-H_2)]$^+$ moiety according to the donor–acceptor interaction analysis. Figure 11 shows that the formate ion part of **10** is remote from the Ru(η^2-H_2) moiety, and the low electron density between Ru(η^2-H_2)···O suggests that the interaction is highly ionic. The high degree of electron localization and the resulting ionic interactions between Ru^+ or Ru(η^2-H_2)$^+$ and the formate ion through the pathways are likely the key factors and characteristic of the reaction.

Overall reaction pathway and towards rational catalyst design: One of the most direct approaches to improve catalytic systems by theoretical means is the search for catalysts capable of lowering the highest activation energy resulting in the rate-limiting step of a reaction. Scheme 3 shows the

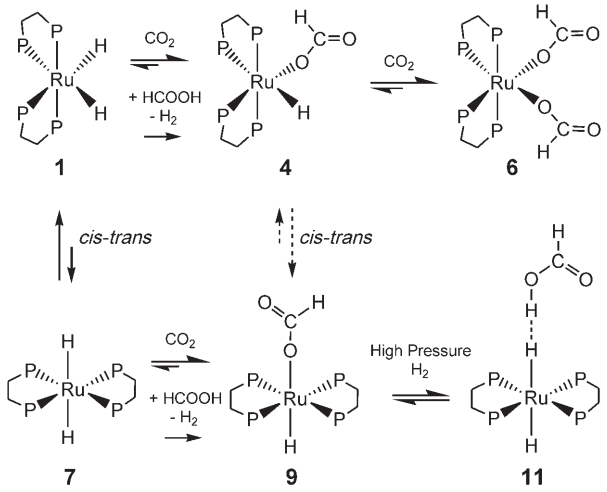

Scheme 3. Main reaction pathways based on experimental and theoretical results. Note that complex **4** was not observed experimentally.

main reaction pathways based on our experimental and theoretical results, and Table 2 summarizes the activation energy required for each reaction event. Overall, the *trans* route shows smaller barriers for forward and backward reactions, and H_2 insertion is the rate-limiting step. Since the "formate ion"-like species are more prominently recognizable at the transition states, the stability of "formate ion" in the vicinity of "Ru^+" or "Ru(η^2-H_2)$^+$" may influence the height of the activation barriers. This hypothesis is supported by the positive charges on H(2) in Table 2 at the transition states (**TS_{8-9}**, **TS_{9-10}**) for the *trans* route, which indicate

Table 2. Activation energies for CO_2 insertion/dissociation and HCOOH reaction/H_2 insertion obtained theoretically. The energies in parenthesis take BSSE correction into account.

Process	Substrate	E_a [kcal mol^{-1}]
CO_2 insertion	*cis*-[Ru(dmpe)$_2$H$_2$]	11.7 (8.7)
	cis-[Ru(dmpe)$_2$H(OCHO)]	11.9 (8.7)
	trans-[Ru(dmpe)$_2$H$_2$]	9.6 (6.4)
CO_2 dissociation	*cis*-[Ru(dmpe)$_2$H(OCHO)]	23.6
	cis-[Ru(dmpe)$_2$(OCHO)$_2$]	19.4
	trans-[Ru(dmpe)$_2$H(OCHO)]	19.2
substitution of hydride by formate	*cis*-[Ru(dmpe)$_2$H$_2$]	26.6 (23.8)
	trans-[Ru(dmpe)$_2$H$_2$]	17.7 (15.1)
H_2 insertion	*cis*-[Ru(dmpe)$_2$H(OCHO)]	26.4
	trans-[Ru(dmpe)$_2$H(OCHO)]	25.4

that electrons flowed into the formate part to stabilize it as the ion. The binding energy of the formate group to the Ru center of some Ru complexes with different ligands, taking Ru^+ and formate ion as reference, showed a "low binding energy/high activity" relation.[31] Therefore, we can attribute the origin of the activation barriers to the ionic interaction strength of the formate unit with the Ru center.

Note that formed formic acid can easily react with the catalytic dihydride complex via dihydrogen-bonding interaction (**11**), and the original formate species are regenerated. A similar interconversion of CO_2/H_2 and formic acid has been reported via dihydrogen bonding and η^2-H_2 complexes,[47–49] and therefore the reversibility of this reaction path is not surprising. Table 2 also indicates that the reaction of formic acid with RuH_2 (i.e., the substitution of hydride by formate) occurs more easily than H_2 insertion into the formate complexes. This has important implications in the catalytic process. In practice, base is added to form a complex product with formic acid and remove it from the catalyst, but the application of amine-like bases make the process less practical for formic acid production. One possibility to avoid using such a base is to use a more polar solvent in which formic acid can dissolve. However, in general H_2 is much less soluble in polar solvents,[50] and therefore the required high H_2 partial pressure cannot be realized. A breakthrough may be realized not only by catalyst design, for example, by engineering and fine-tuning of the ligands, but more promisingly by design of the whole catalytic system, such as a binary or ternary phase catalytic system satisfying the prerequisite of high H_2 concentration near the catalyst, or a continuous reaction, ideally in supercritical CO_2 because of the high solubility of H_2 in that medium, with immobilized catalysts at a higher temperature so that formic acid can be desorbed without base.

Furthermore, we observed greater amounts of *trans* complexes under high H_2 pressure in the presence of some CO_2 (Figures 2 and 5). The equilibrium shift towards *trans* is much faster than the reported *cis–trans* isomerization of the dihydride complex.[28] This fact may be related to the exclusive observation of the *trans* formate complex after reaction of formic acid with RuH_2. When the *cis* and *trans* dihydrogen-bonded complexes are formed, the resulting formic acid can react backwards with the hydride. The equilibrium is suggested to be very fast and expected to shift towards *trans* on reaction with formic acid. The configurational change to *trans* likely takes place under reaction conditions. The abundance of *trans* complexes under high H_2 pressure also supports that the reaction proceeds preferably via the *trans* route.

Conclusion

Combined high-pressure spectroscopic and theoretical investigations have shed light on the detailed reaction and interaction mechanisms during CO_2 hydrogenation with [Ru(dmpe)$_2$H$_2$]. Feasible reaction pathways were suggested by DFT calculations by connecting the species identified by high-pressure IR and NMR studies as being relevant to actual catalytic conditions. The theoretically suggested pathways and energetic stability of the complexes fully support the experimental observations. Several new aspects of the reaction mechanisms are clarified. The Ru–H bond of the dihydride complex is nearly broken when CO_2 interacts with the hydride. Facile CO_2 insertion and the formation of formate complexes then take place in a concerted fashion of two events: Ru–H bond breaking and Ru–O bond formation. Apparently, the insertion step can be viewed as the outcome of rotating "formate ion" near the Ru center. Insertion of H_2 into the formate complexes occurs when the formate group, seemingly present as "formate ion", is far from the Ru center. This step is assigned as the rate-limiting step, and this explains the experimentally observed rate dependence on H_2 pressure. The fact that the dihydrogen-bonded complex between formic acid and the dihydride complex could only be observed under high H_2 pressure supports the assignment. Insertion of H_2 occurs via Ru(η^2-H_2) complexes. An NBO analysis clarified that the complex is relatively stable due to "synergistic H_2 coordination", and the apparent formate ion interacts weakly with the molecular hydrogen coordinated to the Ru center. The stability of formate ion near Ru^+ or $Ru(\eta^2\text{-}H_2)^+$ seems to play a key role in the activation process. Furthermore, formic acid easily reacts with the dihydride complex to form only *trans* formate complex and H_2. The high reactivity likely originates from the stronger dihydrogen bonding and the lower energetic barrier via the *trans* route, as well as the stability of the *trans* formate complex. This step must be carefully considered in designing the actual catalytic system, that is, how should formic acid be extracted from the vicinity of the catalytically active complex. Finally, the *trans* route shows lower activation barriers for all the reaction steps and is likely the dominant pathway of the reaction.

Experimental Section

Materials and synthesis: All reactions and manipulations involving hydride complexes and 1,2-bis(dimethylphosphino)ethane (dmpe, >98%, ABCR) were performed under argon atmosphere by employing standard Schlenk techniques. Toluene (> 99.7%, Fluka) was freshly distilled from sodium/benzophenone under argon prior to use. The dmpe ligand, [(Ru(PPh$_3$)$_3$Cl$_2$] (>99%, ABCR), and deuterated toluene (>99.6%, Eurisotop) were used as received. [Ru(dmpe)$_2$Cl$_2$] was prepared according to the literature[51] from [Ru(PPh$_3$)$_3$Cl$_2$] (6.33 g, 6.60 mmol) and 1,2-bis(dimethylphosphino)ethane (2.0 g, 13.3 mmol) to give [Ru(dmpe)$_2$Cl$_2$] (2.78 g, > 88%) as a pale yellow solid. Approximately 5 g of freshly cut sodium metal was added in small pieces to a solution of [Ru(dmpe)$_2$Cl$_2$] (0.21 g, 0.527 mmol) in dry toluene (30 mL). The mixture was stirred moderately at 313 K, while the reaction vessel was kept inert by a constant slow argon flow (>99.999%, PanGas). Through a septum, a syringe needle was inserted into the solution and hydrogen gas (>99.999%, PanGas) was bubbled through the solution at a constant slow flow rate. This setup was maintained for 60 h while the color of the solution changed from yellow to dark, slightly purple, translucent. To avoid excessive loss of solvent through evaporation, a reflux condenser was attached to the outlet of the vessel. The toluene solution of [Ru(dmpe)$_2$H$_2$] was

then removed by a syringe with a filter to remove the dark precipitate, and an almost colorless, yellowish, clear solution was obtained. All subsequent manipulations and spectroscopic experiments were performed rapidly and without exposing the solution to air. This whole procedure was repeated before each spectroscopic measurement. CO_2 (>99.9993%, Linde AG) and formic acid (>99%, Acros Organics) were used to investigate the reactions with $[Ru(dmpe)_2H_2]$. **Safety note**: The NMR and IR experiments involving elevated pressure require special diligence and appropriate high-pressure equipment, particularly while working with hydrogen gas. For the high-pressure NMR experiments, purpose-built sapphire NMR tubes were used, accompanied by a safety metal container during filling the tube.

Spectroscopic methods: The NMR measurements were performed on a Bruker DRX-400 spectrometer; ^1H, ^{13}C, and ^{31}P chemical shifts were referenced to TMS and 85% H_3PO_4, respectively. For high gas pressures up to 10 MPa, sapphire NMR tubes (∅ 10 mm) were used.[52,53] The spectra were analyzed by WINNMR and fitted using NMRICMA 2.8 (nonlinear least-squares iterative fitting application for MATLAB[54]).

High-pressure IR spectra were obtained by using a home-made batch cell located in a Bruker IFS-66 spectrometer equipped with a liquid-nitrogen-cooled MCT detector with the capability of both transmission and ATR IR measurements up to 200 bar, as well as monitoring sample phases within the cell.[55] A ZnSe crystal was used as the internal reflection element. The angle of incidence and the number of active reflections were 60° and 3, respectively. IR spectra were recorded at 1 cm^{-1} resolution.

Computational methods: Geometry optimization, single-point energy, and harmonic vibrational frequency calculations were performed with the B3PW91 hybrid functional[56,57] using Gaussian 03.[58] A 6-311G(d,p) basis set was applied for all the atoms except Ru. For Ru, the LanL2DZ effective core potential (ECP) basis set was used. The ECP replaces the core electrons of Ru up to 3d and the valence electrons are described by a (341/321/31) basis set.[59] Each transition state was identified with one imaginary frequency and the corresponding normal mode connecting the reaction pathway. Basis set superposition error (BSSE) was corrected by counterpoise approximation[60] when necessary. All calculations were performed as an isolated gas-phase molecule or complex without solvent effects. IR spectra are shown as the sum of Lorentzian lines taking the calculated IR intensity of a normal mode as the height at each frequency. Bonding properties were characterized by natural bond orbital (NBO) analysis.[34,37] Important bond lengths, bond angles, natural bond orders, natural charges, and natural electron configurations are given in the Supporting Information.

Acknowledgements

We thank Dr. R. N. Perutz for his kind advice on the synthesis of $[Ru(dmpe)_2H_2]$, Dr. H. Rüegger for the 2D ^1H–^{31}P correlation analysis, and Dr. D. Ferri, Dr. J.-D. Grunwaldt, and Dr. M. Caravati for fruitful discussions and experimental supports. Computational time at CSCS, Manno, Switzerland and financial support by the Foundation Claude and Giuliana and Swiss National Science Foundation (G.L.) are kindly acknowledged.

[1] *Climate Change 2001: The Scientific Basis*, Cambridge University Press, **2001**.
[2] *Kyoto Protocol to the United Nations Framework Convention on Climate Change*, Kyoto, **1997**.
[3] B. Clark, R. York, *Theory and Society* **2005**, *34*, 391–428.
[4] H. Arakawa, M. Aresta, J. N. Armor, M. A. Barteau, E. J. Beckman, A. T. Bell, J. E. Bercaw, C. Creutz, E. Dinjus, D. A. Dixon, K. Domen, D. L. DuBois, J. Eckert, E. Fujita, D. H. Gibson, W. A. Goddard, D. W. Goodman, J. Keller, G. J. Kubas, H. H. Kung, J. E. Lyons, L. E. Manzer, T. J. Marks, K. Morokuma, K. M. Nicholas, R. Periana, L. Que, J. Rostrup-Nielson, W. M. H. Sachtler, L. D. Schmidt, A. Sen, G. A. Somorjai, P. C. Stair, B. R. Stults, W. Tumas, *Chem. Rev.* **2001**, *101*, 953–996.
[5] W. Leitner, *Coord. Chem. Rev.* **1996**, *153*, 257–284.
[6] A. Baiker, *Appl. Organomet. Chem.* **2000**, *14*, 751–762.
[7] I. Omae, *Catal. Today* **2006**, *115*, 33–52.
[8] M. Aresta, A. Dibenedetto, *Catal. Today* **2004**, *98*, 455–462.
[9] B. Jezowska, P. Sobota, *J. Organomet. Chem.* **1974**, *80*, C27-C28.
[10] Y. Inoue, H. Izumida, Y. Sasaki, H. Hashimoto, *Chem. Lett.* **1976**, 863–864.
[11] E. Graf, W. Leitner, *J. Chem. Soc. Chem. Commun.* **1992**, 623–624.
[12] J. C. Tsai, K. M. Nicholas, *J. Am. Chem. Soc.* **1992**, *114*, 5117–5124.
[13] W. Leitner, E. Dinjus, F. Gassner, *J. Organomet. Chem.* **1994**, *475*, 257–266.
[14] P. G. Jessop, T. Ikariya, R. Noyori, *Nature* **1994**, *368*, 231–233.
[15] P. G. Jessop, Y. Hsiao, T. Ikariya, R. Noyori, *J. Am. Chem. Soc.* **1996**, *118*, 344–355.
[16] Y. Inoue, Y. Sasaki, H. Hashimoto, *J. Chem. Soc. Chem. Commun.* **1975**, 718–719.
[17] P. G. Jessop, Y. Hsiao, T. Ikariya, R. Noyori, *J. Am. Chem. Soc.* **1994**, *116*, 8851–8852.
[18] P. G. Jessop, T. Ikariya, R. Noyori, *Science* **1995**, *269*, 1065–1069.
[19] O. Kröcher, R. A. Köppel, A. Baiker, *Chem. Commun.* **1997**, 453–454.
[20] Y. Musashi, S. Sakaki, *J. Am. Chem. Soc.* **2000**, *122*, 3867–3877.
[21] Y. Y. Ohnishi, T. Matsunaga, Y. Nakao, H. Sato, S. Sakaki, *J. Am. Chem. Soc.* **2005**, *127*, 4021–4032.
[22] F. Hutschka, A. Dedieu, M. Eichberger, R. Fornika, W. Leitner, *J. Am. Chem. Soc.* **1997**, *119*, 4432–4443.
[23] C. A. Thomas, R. J. Bonilla, H. Yong, P. G. Jessop, *Can. J. Chem.* **2001**, *79*, 719–724.
[24] Y. M. Yu, Y. P. Zhang, J. H. Fei, X. M. Zheng, *Chin. J. Chem.* **2005**, *23*, 977–982.
[25] M. K. Whittlesey, R. N. Perutz, M. H. Moore, *Organometallics* **1996**, *15*, 5166–5169.
[26] P. G. Jessop, F. Joó, C. C. Tai, *Coord. Chem. Rev.* **2004**, *248*, 2425–2442.
[27] P. Meakin, Muettert. El, J. P. Jesson, *J. Am. Chem. Soc.* **1973**, *95*, 75–88.
[28] L. D. Field, T. W. Hambley, B. C. K. Yau, *Inorg. Chem.* **1994**, *33*, 2009–2017.
[29] E. S. Shubina, N. V. Belkova, A. N. Krylov, E. V. Vorontsov, L. M. Epstein, D. G. Gusev, M. Niedermann, H. Berke, *J. Am. Chem. Soc.* **1996**, *118*, 1105–1112.
[30] Y. Musashi, S. Sakaki, *J. Am. Chem. Soc.* **2002**, *124*, 7588–7603.
[31] A. Urakawa, M. Iannuzzi, J. Hutter, A. Baiker, *Chem. Eur. J.*, **2007**, submitted.
[32] D. M. Heinekey, M. H. Voges, D. M. Barnhart, *J. Am. Chem. Soc.* **1996**, *118*, 10792–10802.
[33] A. Vigalok, Y. BenDavid, D. Milstein, *Organometallics* **1996**, *15*, 1839–1844.
[34] G. J. Kubas, *Metal Dihydrogen and σ-Bond Complexes*, Kluwer Academic Publishers, New York, **2001**.
[35] G. J. Kubas, *Catal. Lett.* **2005**, *104*, 79–101.
[36] P. Munshi, A. D. Main, J. C. Linehan, C. C. Tai, P. G. Jessop, *J. Am. Chem. Soc.* **2002**, *124*, 7963–7971.
[37] E. D. Glendening, J. K. Badenhoop, A. E. Reed, J. E. Carpenter, J. A. Bohmann, C. M. Morales, F. Weinhold, NBO 5.0, Theoretical Chemistry Institute, University of Wisconsin, Madison, **2001**.
[38] F. Weinhold, C. Landis, *Valency and Bonding*, Cambridge University Press, **2005**.
[39] M. T. Bautista, E. P. Cappellani, S. D. Drouin, R. H. Morris, C. T. Schweitzer, A. Sella, J. Zubkowski, *J. Am. Chem. Soc.* **1991**, *113*, 4876–4887.
[40] C. A. Sandoval, T. Ohkuma, K. Muniz, R. Noyori, *J. Am. Chem. Soc.* **2003**, *125*, 13490–13503.
[41] S. E. Clapham, A. Hadzovic, R. H. Morris, *Coord. Chem. Rev.* **2004**, *248*, 2201–2237.
[42] Y. Nishibayashi, I. Takei, M. Hidai, *Angew. Chem.* **1999**, *111*, 3244–3247; *Angew. Chem. Int. Ed.* **1999**, *38*, 3047–3050.
[43] I. Takei, Y. Nishibayashi, Y. Ishii, Y. Mizobe, S. Uemura, M. Hidai, *J. Organomet. Chem.* **2003**, *679*, 32–42.

[44] R. Custelcean, J. E. Jackson, *Chem. Rev.* **2001**, *101*, 1963–1980.
[45] G. Orlova, S. Scheiner, T. Kar, *J. Phys. Chem. A* **1999**, *103*, 514–520.
[46] E. I. Gutsul, N. V. Belkova, M. S. Sverdlov, L. M. Epstein, E. S. Shubina, V. I. Bakhmutov, T. N. Gribanova, R. M. Minyaev, C. Bianchini, M. Peruzzini, F. Zanobini, *Chem. Eur. J.* **2003**, *9*, 2219–2228.
[47] H. S. Chu, C. P. Lau, K. Y. Wong, W. T. Wong, *Organometallics* **1998**, *17*, 2768–2777.
[48] Y. F. Lam, C. Q. Yin, C. H. Yeung, S. M. Ng, G. C. Jia, C. P. Lau, *Organometallics* **2002**, *21*, 1898–1902.
[49] M. L. Man, Z. Y. Zhou, S. M. Ng, C. P. Lau, *Dalton Trans.* **2003**, 3727–3735.
[50] *Solubility Data Series*, *Vol. 5/6*, Pergamon Press, Oxford, **1985**.
[51] L. D. Field, A. V. George, G. R. Purches, A. H. White, *J. Chem. Soc. Dalton Trans.* **1996**, 2011–2016.
[52] A. Cusanelli, U. Frey, D. T. Richens, A. E. Merbach, *J. Am. Chem. Soc.* **1996**, *118*, 5265–5271.
[53] G. Laurenczy, F. Joó, L. Nadasdi, *Inorg. Chem.* **2000**, *39*, 5083–5088.
[54] The MathWorks, MATLAB ver. 6.5.
[55] M. S. Schneider, J. D. Grunwaldt, T. Bürgi, A. Baiker, *Rev. Sci. Instrum.* **2003**, *74*, 4121–4128.
[56] A. D. Becke, *J. Chem. Phys.* **1993**, *98*, 5648–5652.
[57] J. P. Perdew, Y. Wang, *Phys. Rev. B* **1992**, *45*, 13244–13249.
[58] Gaussian 03, revision C.02, M. J. Frisch, G. W. Trucks, H. B. Schlegel, G. E. Scuseria, M. A. Robb, J. R. Cheeseman, J. A. Montgomery, Jr., T. Vreven, K. N. Kudin, J. C. Burant, J. M. Millam, S. S. Iyengar, J. Tomasi, V. Barone, B. Mennucci, M. Cossi, G. Scalmani, N. Rega, G. A. Petersson, H. Nakatsuji, M. Hada, M. Ehara, K. Toyota, R. Fukuda, J. Hasegawa, M. Ishida, T. Nakajima, Y. Honda, O. Kitao, H. Nakai, M. Klene, X. Li, J. E. Knox, H. P. Hratchian, J. B. Cross, C. Adamo, J. Jaramillo, R. Gomperts, R. E. Stratmann, O. Yazyev, A. J. Austin, R. Cammi, C. Pomelli, J. Ochterski, P. Y. Ayala, K. Morokuma, G. A. Voth, P. Salvador, J. J. Dannenberg, V. G. Zakrzewski, S. Dapprich, A. D. Daniels, M. C. Strain, O. Farkas, D. K. Malick, A. D. Rabuck, K. Raghavachari, J. B. Foresman, J. V. Ortiz, Q. Cui, A. G. Baboul, S. Clifford, J. Cioslowski, B. B. Stefanov, G. Liu, A. Liashenko, P. Piskorz, I. Komaromi, R. L. Martin, D. J. Fox, T. Keith, M. A. Al-Laham, C. Y. Peng, A. Nanayakkara, M. Challacombe, P. M. W. Gill, B. Johnson, B. Chen, M. W. Wong, C. Gonzalez, J. A. Pople, Gaussian Inc. Pittsburgh, PA.
[59] P. J. Hay, W. R. Wadt, *J. Chem. Phys.* **1985**, *82*, 299–310.
[60] S. F. Boys, F. Bernardi, *Mol. Phys.* **1970**, *19*, 553.

Received: September 18, 2006
Published online: February 12, 2007

